Soft Matter

Accepted Manuscript

ROYAL SOCIETY OF CHEMISTRY

www.rsc.org/softmatter

Cite this: DOI: 10.1039/c0xx00000x

www.rsc.org/xxxxxx

ARTICLE TYPE

Adsorption of Rationally Designed "Surf-tides" to a Liquid-Crystal Interface

Joseph V. Badami,[a] Chaim Bernstein,[a] Charles Maldarelli,[a] Raymond S. Tu*[a]

Received (in XXX, XXX) Xth XXXXXXXXX 20XX, Accepted Xth XXXXXXXXX 20XX
DOI: 10.1039/b000000x

The interfacial adsorption of proteins in surfactant laden systems occurs both in nature and industrial processing, yet much of the fundamental behavior behind these mechanisms is still not well understood. We report the development of a system that monitors optical transitions of a liquid-crystalline/aqueous interface to examine the dynamics of adsorption of two rationally designed model peptide molecules. The two molecules synthesized in this study were both designed to become surface-active upon folding and contain the same net charge of +3, but one of the peptides, K-2.5, has its three charges separated by 2.5 amino acids as compared to K-6.0, which has its three charges separated by 6 amino acids. Our study examines the roles that charge distribution and secondary structure have on the relative adsorption dynamics of these two models peptides onto a fluid/fluid interface. Using the optical detection of molecular adsorption and image analysis of these events, we obtain quantitative information about the dynamics as a function of the charge spacing and initial peptide concentration. We show that both peptides initially follow a diffusion-limited adsorption model onto the interface. Additionally, our results suggest that the K-6.0 peptides demonstrate enhanced adsorption kinetics, where the enhanced rates are a consequence of the well-folded adsorbed state and spatial distribution on the surface. These findings provide further insights into the role that charge spacing has on secondary structure and subsequently the dynamics of adsorption, while developing a versatile system capable of extracting quantitative information from a simple inexpensive optical system.

Introduction

This study describes the application of liquid-crystalline (LC) materials to visualize the dynamics of biomolecular adsorption and interfacial self-assembly at the LC/aqueous interface. LC materials are well-suited for the characterization of interfacial behavior as they undergo cooperative long-range ordering in response to external surface stimuli. Moreover, the ordering results in an easily visualized change in the polarization state, allowing LC-based systems to be readily commercialized [1]. The long-range, orientational dynamics can be examined as a function of the surface activity of the adsorbates [2]. These LC materials possess degrees of anisotropy that result in distinct macroscale characteristics, including viscoelastic behavior and diamagnetic/dielectric properties [3]. Most importantly for the work described here, this anisotropy yields changes in refractive indices leading to complex interactions (i.e. birefringence) with incident light not seen in isotropic fluids while still maintaining fluid-like behavior [4].

More recently, the application of nematic LCs in contact with aqueous phases to serve as a model oil/aqueous interface has allowed for the optical examination of the adsorption of surfactants [5], lipids [6], polymers [7], nucleic acids [8], and proteins [9]. The configurations simultaneously permit the development of highly complex assemblies consisting of several discrete layers that mimic naturally occurring (i.e. outer membrane leaflets) [10] or synthetic (i.e. hydrogel/external environment) [11] interfaces, while providing optical amplification of molecular events. Additionally, such systems allow for the transduction of highly specific molecular interactions including ssDNA complement interactions [12], enzymatic "lock and key" activity [13], aptamer pairing [14], and protein receptor-ligand binding [15].

Figure 1 illustrates the experimental setup, where a LC-filled electron microscopy specimen grid is placed in contact with a hydrophobically functionalized glass microscope slide. Previously, Nazarenko et al. detailed findings of orientational effects of freely suspended LC in contact with air, following contact with a copper foil substrate [16]. Their experiments concluded that upon heating above the nematic-isotropic phase transition temperature, slower cooling rates (>100s) led to homeotropic (LC molecular long-axis perpendicular to the surface) alignment, while faster rates (<40s) promoted a planar (LC molecular long axis parallel to the interface) surface. Thereafter, Brake et al. expanded upon these findings by developing a setup for examining the adsorption of surfactants to fluid/fluid interfaces (as described above) that eliminated several experimental issues (i.e. curved surfaces, LC dewetting) by confining the LC within a specimen grid via capillary forces [17]. The work from the Abbott lab highlighted three key advantages of this configuration. First the LC can be directly visualized, allowing for the "label-free" characterization of adsorption at a fluid/fluid interface using only a polarized light microscope.

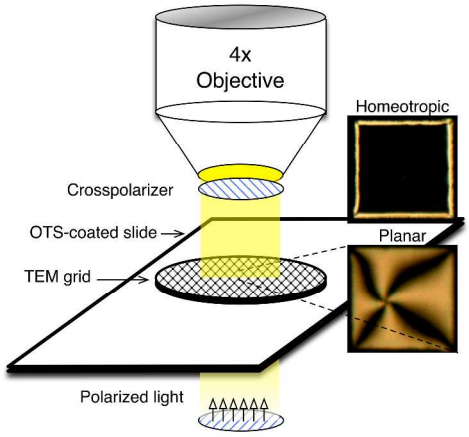

Figure 1. Experimental polarized light microscopy optical cell as previously described by Brake et al. consisting of a liquid crystal filled specimen grid seated on a hydrophobically functionalized (C18 acyl chain) glass slide immersed in an aqueous (solute-containing) phase.

Additionally, this also negates the requirement of expensive, complex instrumentation commonly used in interfacial measurements (i.e. Langmuir trough, Pendant drop/bubble apparatus, Ellipsometry, Quartz Crystal Microbalance) while providing a possible means for cheap, "in-field", point-of-care sample analysis. Second, the fluidity of the interface inherently allows for the lateral diffusion of molecules following adsorption to the surface. Third, the reversibility of these adsorption processes is also easily detectable. Capturing the dynamics of adsorption in model peptide systems as a function of secondary structure is the focal point of our present study.

We present several experiments that visualize both the equilibrium behavior and adsorption dynamics of two rationally designed peptides at a surfactant-laden, LC/aqueous interface. In this system, the "competitive adsorption" of the peptide-surfactant systems reflects the physico-chemical properties (i.e. solubility, surface-activity) of the mixture components [18]. Work from Rodriguez et al. describes two experimental permutations for multi-component systems to adsorb: (i) direct adsorption of a multi-component mixture to a clean interface and (ii) sequential penetration onto and/or displacement of material from a pre-formed surfactant layer [19]. Our present study exploits the latter adsorption mechanism where our model peptides penetrate/displace a pre-formed surfactant layer, allowing us to examine the role of charge distribution on the non-specific, adsorption dynamics. These peptide molecules demonstrate our ability to advance this technology towards the incorporation of specific interactions for protein/peptide-based bio-sensing applications.

Experimental Section

Materials

Peptides (K-2.5 and K-6.0, >90% purity) were obtained from Anaspec, Inc. (Fremont, CA, USA). Synthesis and purification were confirmed by mass spectrometry and high-performance liquid chromatography. Cetyl trimethylammonium bromide (CTAB, 99+% purity) surfactant, Octadecyltrichlorosilane (OTS), and 4-cyano-4′-pentylbiphenyl (5CB, >98% purity) nematic liquid crystal were obtained from Sigma-Aldrich (St. Louis, MO). Plain Gold Seal glass slides (Portsmouth, N.H.) and Lab-Tek II Chamber Slides (8-well) were purchased from Fisher Scientific (NJ, USA). Sulfuric acid and Nochromix (Godax Laboratories Inc., MD, USA) were obtained from Sigma-Aldrich (St. Louis, MO). All solutions were prepared with filtered, deionized water to a resistivity of 18.2 MΩ (Direct-Q, Millipore, Billerica, MA). Sodium Chloride (NaCl), Ethanol, Methanol, Heptane, and Methylene Chloride were obtained from Fisher Scientific (NJ, USA). Copper specimen grids (75 mesh, 283 μm hole size, 50 μm bar width) were purchased from Electron Microscopy Sciences (Hatfield, PA, USA).

Peptide Design

The design of the two rationally designed peptides used in these experiments was discussed in detail previously [20]. Briefly, both model molecules were designed to examine the role of charge distribution along the peptide backbone on both secondary structure and surface activity. Our design methodology follows two well-cited design 'rules': intrinsic propensity and periodicity [21-23]. The combination of these design rules provide a framework for de novo design of a well-nucleated secondary structure. Previously, our group has used these rules in the successful design of both surface-active α-helical and β-sheet peptides [24-28].

Both molecules used in this study are composed of the same 22 amino acids and therefore, both molecules possess the same molecular weight (MW = 2405.9 g/mol). They both consist of an equal number of alanine (A), leucine (L), lysine (K), glutamine (Q), and glutamic acid (E). The two sequences, K-2.5 (E-LAQQALK-LAKQALK-LAQQALK) and K-6.0 (E-LAQKALQ-LAKQALQ-LAQKALK) differ only in the spacing of positively charged lysine residues along the backbone (Figure 2). With the goal of constructing α-helical peptides, our sequences contain amino acids with high helical propensities and periodic placement of hydrophobic residues in order to promote an α-helical architecture. Additionally, upon folding the sequencing of amino acids leads to an alignment of hydrophilic residues (lysine, glutamine, and glutamic acid) isolated to one face of the cylinder's polar axis and hydrophobic residues (alanine and leucine) situated on the opposing face. Therefore, both peptides become surfactant-like along the longitudinal axis of the molecule.

Circular Dichroism – Secondary Structure Analysis

Characterization of peptide secondary structure as a function of electrolyte (NaCl) concentration was determined using circular dichroism (CD) spectroscopy. Scans were performed over the range of 190-250 nm using an Olis DSM 20 spectrophotometer (Olis, Bogard, GA). Cylindrical cuvettes (1.0 mm path length, quartz) were used and results presented are the average of a minimum ten scans at room temperature. Output from the instrument was given in units of millidegrees, θ. Conversion to normalized units [deg cm^2 $dmol^{-1}$] of mean residue ellipticity (MRE, $[\theta]_{MRE}$) was done using the following relation, $[\theta]_{MRE} = 100*\theta/(c*l*n)$, where θ is the instrument output in millidegrees, c is the molar concentration, and l is the path length (cm.), and n is the number of amino acids in the protein/peptide sequence.

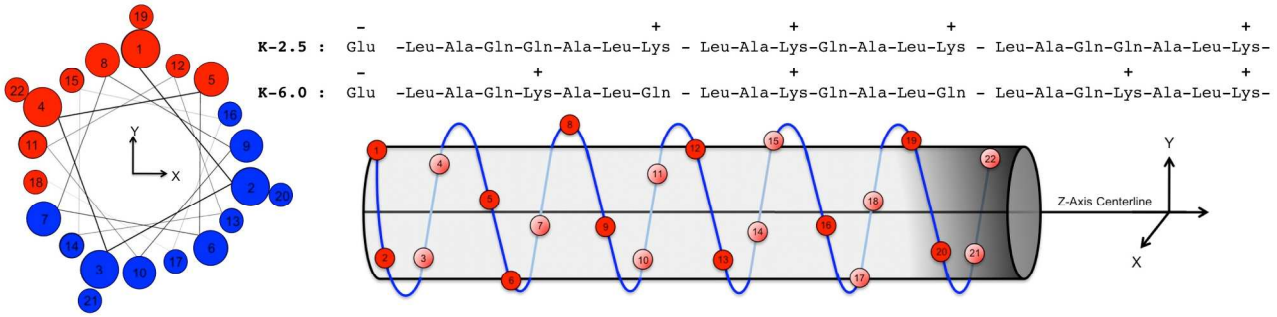

Figure 2. Peptide K-2.5 and K-6.0 sequences with numbered amino acid positions and charged residue distribution. Left: Helical wheel depiction illustrating amphiphilic molecular architecture (hydrophilic = red and hydrophobic = blue). Right: Long axis schematic depicting relative amino acid positions along helix upon folding. Residues above the centerline (positive Y) hydrophilic and below (negative Y) hydrophobic.

Formation of Optical Cells

Glass slides were cleaned by immersion in a solution of Nochromix and 98% sulfuric acid overnight. The remainder of the procedure was followed as previously described by Brake et al. [17]. Briefly, the slides were removed from the Nochromix solution and rinsed successively in deionized water, ethanol, and methanol. They were then dried under a stream of nitrogen gas, followed by heating to ~110°C in an oven and left overnight. Slides were then immersed in a solution of 0.5 mM OTS in heptane at room temperature for 30 minutes. Lastly, they were then rinsed with methylene chloride and dried by a stream of gaseous nitrogen prior to use.

Copper specimen grids were first cleaned with methanol and dried under gaseous nitrogen. Grids were then placed on top of OTS treated glass slides and contacted with 2 µL of 5CB liquid crystal. A glass capillary tube was then used to remove excess 5CB from the surface by contacting the interface, leaving a flat film deposited within the square spaces of the grid as described previously [17]. The liquid-crystal containing grid was then heated above the nematic-isotropic transition temperature (35°C) to remove any remaining stresses induced by the impregnation of 5CB into the copper grid. Upon cooling below this transition temperature, cells were visualized by optical microscopy (4x magnification) under crossed polarizers to detect homoetropic anchoring of the LC. Any slides not exhibiting such orientation were immediately discarded and eliminated from further usage. Grids were positioned centrally in of eight-well chamber slides as described previously by Price et al. [12].

LC/Aqueous Interface, Monolayer Preparation, and Peptide Addition

For the experiments investigating the orientational effects of proteins/peptides on the pure LC/aqueous interface, 200 µL of 100 mM NaCl solution was introduced into the well to completely immerse the TEM grid. After allowing the system to equilibrate (10-15 min.) and take on a planar orientation (Figure 3a), 10 µL of the peptide solutions of at various concentrations were added to the system. Once again the system was allowed to equilibrate until no further changes to the LC orientation was observed.

Experiments conducted using an LC/Aqueous-CTAB interface followed the same procedure. First, 200 µL of 0.01 mM CTAB in 100 mM NaCl was added to the well and allowed to reach equilibrium (10-15 min.). Conversely, the presence of the straight-chain carbon tail of the CTAB molecule promotes a homeotropic orientation of the LC interface (Figure 3b). Any grids not showing such orientation in contact with CTAB were eliminated. Protein/peptide solutions were similarly added in 10 µL volumes and allowed to reach equilibrium (Figure 3c). Bulk peptide concentrations used in these experiments ranged from 0.7-0.1 µM (0.37-1.3x10^{-3} g/L). All samples were covered during this period to limit any evaporation of the solutions.

Visualization by Optical Microscopy and Image Analysis

Optical cells containing 5CB were examined in transmission mode using a polarized light microscope (Eclipse 50i , Nikon, Tokyo, Japan). Samples were viewed under crossed polarizers and 4x magnification. Planar and near-planar orientations were observed as colorful, bright regions with the development of brush patterns (i.e. dark regions emanating from the center outwards towards the grid). Upon addition of CTAB, homeotropic alignment was additionally confirmed by a manual sample rotation (90 degrees). Data collection was performed by taking videos and/or time-lapse images at given intervals using a QICAM (QImaging, Model QIC-F-CLR-12). Analysis of images was performed using ImageJ software. The results presented are the mean-intensity values compiled by utilizing a square-by-square approach from a minimum of 12 different squares on a

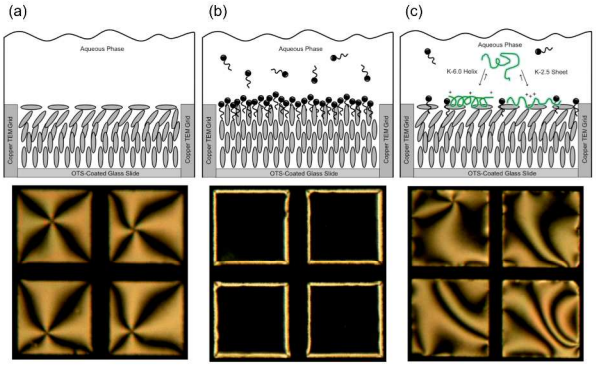

Figure 3. Orientational schematic (Top) and optical (Bottom) configurations of LC (ellipsoids) in contact with aqueous phases. (A) LC in contact with deionized water/NaCl solution (planar orientation) (B) LC in contact with aqueous CTAB solution (homeotropic orientation) (C) LC in contact with CTAB solution followed by peptide addition (tilted/planar orientation).

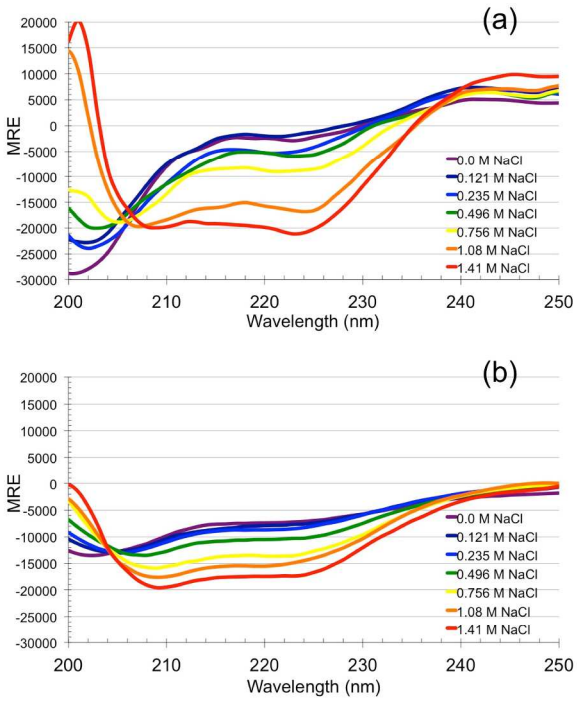

Figure 4. CD spectra as a function of NaCl concentration for (a) K-6.0 and (b) K-2.5.

given TEM grid. For each given concentration, at least five independent TEM grids were examined on a minimum of two different glass slides. Data normalization was performed using the average of the last 10 data points at max-intensity plateau average to account for variations in brush patterning and deviations in microscope configuration such as lamp intensity and focal depth.

Results and Discussion

Multi-component systems consisting of proteins/peptides and surfactants are prevalent in nature [29]. Additionally, combinations of protein-surfactant mixtures serve as the primary stabilizing agents across many industrial applications including the processing of cosmetics, pharmaceuticals, and food products [30], but the quantitative examination of multi-component adsorption reamains technically challenging largely due to the complexity associated with the multiple structural states (i.e. folded/unfolded) inherent in protein-surfactant mixtures. Therefore, the understanding of the interactions of these materials and the interfacial layers they form at surfaces between immiscible phases remains a crucial step in advancing manufacturing protocols. The following results demonstrate a simple and inexpensive tool to evaluate interfacial dynamics in a peptide-surfactant system.

Secondary Structure Analysis via CD

Peptide secondary structure as a function of electrolyte concentration was determined using circular dichroism. Figure 4 shows the spectra for both peptides over the range of 0 – 1.41 M at room temperature. Similar structural transitions are observed for both molecules. As the electrolyte concentration is increased,

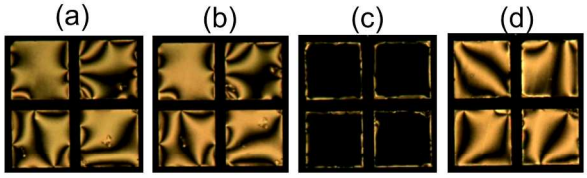

Figure 5. Polarized microscopy images of (a) clean aqueous/LC interface (0.1 M NaCl), (b) aqueous/LC after addition of 0.6 μM K-6.0, (c) surfactant-laden, aqueous/LC interface (0.1 M NaCl and 0.01 mM CTAB) and (d) surfactant-laden, aqueous/LC interface after addition of 0.6 μM K-6.0.

a configurational rearrangement from a random coil (disordered) ensemble average (minima at 198~200 nm) to a majority α-helical ensemble average is observed. These findings were expected as the increase in electrolyte concentration diminishes the electrostatic repulsion amongst neighboring residues along the peptide backbone, subsequently lowering the free energy barrier for folding [26]. Prior to experimentation, GOR4 computational secondary structure prediction was used to assess secondary structure a priori as a function of primary sequence. For both molecules, these predictions yielded 63-65% α-helical and 35-37% random coil. After performing secondary structure analysis by applying least-squares fits of characteristic basis spectra to our CD results, K-2.5 displayed traits of α-helices, β-sheets, and random coil ensemble averages of 25/25/50% in 0M NaCl and 68/23.7/8.3% in 1.41M NaCl, while K-6.0 showed only α-helix and disordered structures of 21/79% in 0M NaCl and 82.1/17.9% in 1.41M NaCl. At 0.1M NaCl (experimental conditions), ensemble averages were found to be 31.9/20/48.1% (α-helix/β-sheet/random coil) for K-2.5 and 23.1/76.9% (α-helix/random coil) for K-6.0. Both peptides show a slight decrease in random coil population as compared to the purely deionized water as expected. Experiments were also conducted to verify that the presence of CTAB at experimental concentrations did not influence the peptide secondary structure. In both cases, the surfactant did not alter the CD spectra and the aforementioned structural averages.

Peptide Adsorption to Aqueous/Liquid-Crystal Interface

Upon addition of peptide to a "clean" (i.e. no surfactant present) aqueous/LC interface, no significant (<5%) changes in mean intensity and only slightly visible changes in brush pattern formation were observed (Figure 5 a-b). These findings for both peptides were consistent with previous studies involving the deposition of higher molecular weight proteins (i.e. BSA, Streptavidin, etc.) to the aqueous/LC interface [9, 15, 31, 32]. The mechanism for this phenomenon was previously investigated by Lockwood et al. in which they studied the orientational effects induced by both linear and branched chain surfactants [5]. They observed that linear, acyl tail surfactants promoted the homeotropic orientation of 5CB at the interface, while branched chain molecules led to planar optical appearance. These findings demonstrate that, in the case of straight-chain molecules, the LC molecular structure is capable of aligning along the same axis as the surfactant. Conversely, branched architecture present in the surfactant structure disrupts this molecular alignment enough at the surface, leading to a planar optical signal.

In the case of the two model peptides examined in this study, we have previously shown that upon binding to an interface, the folded structure is the dominant species [20]. Upon folding, the hydrophobic face contains both alanine and leucine residues, neither of which contains linear acyl chains of significant length. Additionally, the peptide backbone presents torsional angle restrictions down the length of the molecules further limiting an arrangement of hydrophobic side groups that would promote a homeotropic state. Based on these findings, our current study adopts a methodology that exploits this transitional behavior by beginning with a surfactant-laden interface that takes on a homeotropic configuration (Figure 5c) and converts to planar orientation after a sufficient quantity of peptide adsorbs to the interface (Figure 5d).

Prior to the inclusion of peptide to this surfactant-laden surface, control experiments were conducted to ensure that additional buffer solution alone did not alter the optical appearance over the timescales measured in this study. Volumes of 100 μL were added and no change was observed over extended periods of time (~24hr.), indicating that optical transition was indeed peptide-driven. In order to promote the optical transition used throughout this study, the peptide molecules must be able to adsorb to the surface, increasing the mean molecular area via intercalation or displacing the surfactant from the surface. In order to intercalte between adsorbed surfactants, the peptide-suface affinity must be sufficient to overcome the surfactant-surfactant interactions. In contrast, in order to displace the surfactant from the surface, the peptide-surface affinity must be sufficient to overcome the surfactant-liquid crystal interactions. Figure 5 demonstrates that the surfactant-LC interaction is replaced by the peptide-LC interaction. As to whether the peptide displaces the CTAB from the interface or the peptide partitions into the CTAB-laden interface remains unclear. In either case, for the case of sensing applications, the ideal system provides detection of low analyte levels while ensuring a robust platform for obtaining results with high reproducibility.

Initial experiments were conducted using CTAB at a concentration of 0.1 mM (one order of magnitude greater), but no optical transitions were observed at any of the peptide concentrations measured throughout this study (data not shown). All experiments conducted at 0.1 mM surfactant concentration remained in a homeotropic state, illustrating the influence of initial surfactant concentration on the packing density at the surface. Our final setup adopted a concentration of CTAB at 0.01 mM, which we found to be the lowest concentration that provided a reproducible homeotropic initial configuration while allowing for detection of low peptide concentration at the desired electrolyte concentration.

The optical transitions observed arise from a balance of surfactant concentration, electrolyte concentration, and peptide concentration that possesses the potential to be optimized to optically detect predetermined critical concentrations of analyte for the case of bio-sensing. With the goal of increasing the sensitivity (i.e. optically observe adsorption at lower peptide concentrations), the selection of straight-chain surfactant (molecular structure and bulk concentration) and electrolyte concentration remain as the free parameters to be tuned. In this study, ionic surfactants are used, and the areal packing density of surfactant at the interface results from a balance of electrostatic repulsion between the headgroups and hydrophobic attraction between the acyl tails. Varying the initial surfactant bulk concentration leads to differing degrees of interfacial molecular density as the system adjusts to develop a thermodynamic equilibrium, a phenomenon that can readily be visualized by monitoring coloration differences of the LC surface to the point of hometropic alignment and beyond. Moreover, fixing the surfactant concentration and increasing the electrolyte concentration provides an effective means to fine tune the surfactant density by adjusting the Debye length and allowing the headgroups to decrease their mean molecular area. Holding the headgroup constant and varying the acyl tail length allows for an additional parameter in optimization by manipulating the strength of the attractive force between neighboring molecules. Optimizing these aforementioned adjustable parameters allows for the creation of "optical windows" that permit the visualization of analytes within specific concentration ranges for the application at hand.

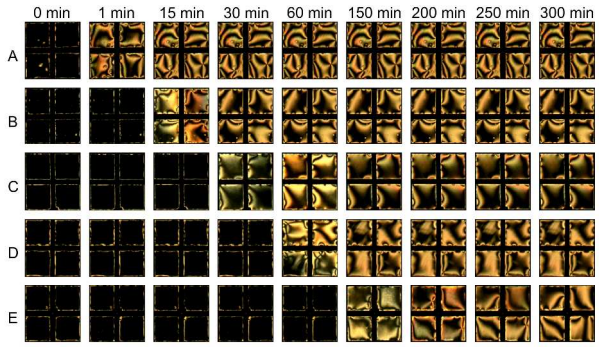

Figure 6. Time-dependent ordering transitions of LC interface upon the addition of K-6.0 peptide to a bulk concentration of (A) 0.7 μM (B) 0.5 μM (C) 0.41 μM (D) 0.31 μM (E) 0.15 μM.

Diffusion limited peptide adsorption

While Figure 5c-d reflects the initial and final equilibrium optical signal that serves as the focus of this work, the dynamics of this transition can also be monitored to gain information about the rates of adsorption of both peptides. Figure 6 shows the optical images that reflect this time-dependent transitional behavior as a function of the quantity of peptide added to the system, simultaneously highlighting initial transition time-points for each concentration. For all cases the system begins with a surfactant-covered surface (homeotropic orientation) and upon the addition of peptide transforms into an optically bright (tilted/planar orientation) surface. As expected, we observed that as the peptide concentration is increased, the time required to establish a planar orientation decreased. The onset of this transition (Figure 6b 15min., Figure 6c 30min., and Figure 6e 150min.) is accompanied by the LC tilting from an orientation normal to the surface to an orientation parallel.

Intermediate changes in color (Figure 6e 200min.) are also capable of providing information as the progression of coloration has previously been corroborated with concentration of surfactant present at the interface [33]. The adsorption of peptides to the surface promoted a progression from darker hues of grey, orange, red and green to brighter saturations of gold, pink, and light green.

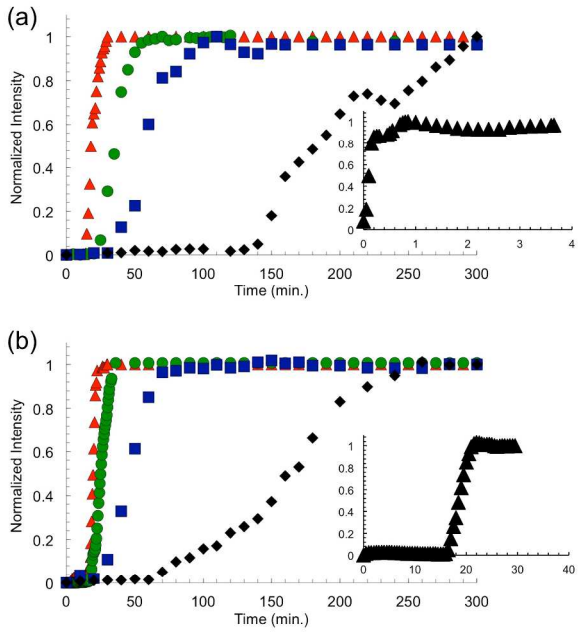

Figure 7. Dynamics of adsorption for (a) K-6.0 and (b) K-2.5 at 0.5 μM (red), 0.41 μM (green), 0.31 μM (blue), and 0.2 μM (red). Inset graphs correspond to adsorption behavior at 0.7μM.

Image analysis shows a sigmoidal increase in the mean intensity until an equilibrium configuration is achieved. As mentioned previously, the aim of this work is to develop this system to investigate the adsorption behavior of two rationally designed peptides of differing charge distribution, visualizing the effect of electrostatics on the dynamics of adsorption. Using time-lapse sequences as shown in Figure 6, normalized intensity curves were obtained for both peptides at five peptide concentrations ranging from 0.15μM, to 0.7μM, Figure 7. In both cases we observe similar behavior. Specifically, a series of sigmoidal curves with two plateaus. The duration of the lower plateau decreases as we increase the peptide concentration. We can quantify this "critical time", t_c, (described further below) when transition begins to take place. Following this critical time point, an increase in intensity is observed until an upper bound is reached. The initialization of the upper plateau corresponds to the point where the system has reached the maximum intensity value and no further optical changes are observed. However, the upper plateau does not necessarily coincide with the system reaching a final equilibrium, as additional peptide is likely still adsorbing to the interface beyond this time point.

Previous work by Hunter et al. reported similar trends using the LC/gas interface as a sensor for the presence of chemical vapor compounds [34]. Their work concluded that the critical transition is defined by a critical surface concentration of vapor that diffused and adsorbed to the interface. In this study, we expect similar behavior where a critical surface concentration of peptide, Γ_c , is required to promote an optical transition. In order to determine Γ_c , we consider the case where our peptides are in a "diffusion-limited" regime. In this regime, the adsorption to the initially peptide-free interface from the sub-layer is fast as compared to the slower diffusion of peptide molecules to the sub-surface layer. In order to justify our assumption, we show that

Peptide	Conc (μM)	t_c(min.)	dI/dt (min^{-1})
K-2.5	0.70	16	0.220
K-2.5	0.50	17	0.200
K-2.5	0.41	18	0.065
K-2.5	0.31	20	0.020
K-2.5	0.15	60	0.005
K-6.0	0.70	0.1	310.0
K-6.0	0.50	14.5	0.117
K-6.0	0.41	20	0.030
K-6.0	0.31	30	0.014
K-6.0	0.15	130	0.009

Table 1. Values of critical times and slopes for both peptides at measured concentrations

for each bulk concentration (C_B) and critical time (t_c), the calculated value of the of the critical surface concentration (Γ_c) is a constant value The values for these concentrations and critical times for both peptides can be seen in Table 1. Using the diffusion-limited, Ward-Tordai expression below, we are able to calculate Γ_c :

$$\Gamma_c \approx 2C_B\sqrt{\frac{Dt_c}{\pi}}$$

where the value for the diffusion coefficient, D, is based on previous work from our group, approximating D by modeling the peptide as a cylinder and validating the approximation with experimental data [25].

Following this analysis, we use a diffusion coefficient for both peptides to be $2\text{x}10^{-10}$ m^2/s. Using the Ward-Tordai equation above with the experimental critical times and bulk concentrations, we found the critical surface concentration for transition, $\Gamma_c = 2.21 \pm .0024\ \text{x}10^{-7}$ mol/m^2. As expected, we found this value to be a constant for all the peptide concentrations investigated in this study, justifying our diffusion-limited analysis.

After determining Γ_c, we extended our analysis to determine if the adsorption rate also followed diffusion-limited behavior, and, more specifically, if the change in intensity with respect to time measured in our experiments (*dI/dt*) was proportional to the change in surface concentration with respect to time (*dΓ/dt*). Taking the derivative of the expression above for the time-dependent surface concentration, the following expression is obtained:

$$\frac{d\Gamma}{dt} \approx C_B\left(\frac{Dt}{\pi}\right)^{-1/2}$$

From this expression, we would expect that the intensity measured in our experiments was proportional to the slopes (dI/dt)~(dΓ/dt), but, after performing this analysis, we found that this relationship does not support the data collected in our experiments. We believe that this relationship does not hold because *dI/dt* is not proportional to *dΓ/dt*.

A possible rationale for why this relationship does not hold is that as the peptides are adsorbing to the surface, this change in intensity is the net result of two processes. First, the peptide is adsorbing in a diffusion-limited manner as detailed from our prior analysis. Second, as the peptide adsorbs to the surface, it is competing for interfacial area with the surfactant that originally

occupied the same area. This competition for surface area may occur via (1) peptide adsorbing to the surface and displacing surfactant from the interface and/or (2) peptide adsorbing to the interface and intercalating into the surfactant layer, inducing an increase in the surface pressure. Elucidating the exact mechanism lies outside the scope of this work, however it is clear that the adsorption of both peptides to the LC surface disrupts the original areal packing density of the surfactant that promotes hometropic orientation at the experimental surfactant concentration.

Comparison of K-2.5 and K-6.0 Adsorption Dynamics

In addition to the quantitative analysis of the adsorption kinetics, we also use the LC system to compare the effect of charge distribution on the adsorption two rationally designed peptides. As mentioned previously, for each peptide the critical time decreased and rate of intensity change increased with increasing peptide concentration, but, comparing the two peptides at the highest concentration measured in our experiments, we observe a distinct difference in both the critical time and the transition intensities (Figure 7a and b, Inset Graphs). K-6.0 promoted a critical time ~10 seconds and steep slope, but K-2.5 showed a critical time of 16 minutes and much slower rate of intensity change.

This critical time for K-6.0 also corresponds to the minimum time required for a resolvable signal to be achieved under these experimental conditions. Taking into consideration that at the experimental conditions circular dichroism analysis confirms that K-2.5 contains a more folded (amphipathic) population (~32%) as compared to K-6.0 (~23%), we believe that at this higher concentration the charge separation influences peptide packing at the liquid crystal interface. Previous work from our group has shown through Langmuir-trough experiments that peptide molecules with more closely spaced charges result in a lower surface pressure across the interface [27, 28]. We have hypothesized that this results from the peptides with a localized charge distribution being able to pack into a staggered structure via intermolecular interactions, as opposed to molecules with more evenly distributed charge locations down the length of the structure.

Once the concentration was lowered to 0.50 μM, K-2.5 had a critical time of 17 min., as compared to 14.5 min. for K-6.0. Conversely, K-2.5 showed a greater rate of intensity change (0.200 min^{-1}) when compared to K-6.0 (0.117 min^{-1}). At this concentration, both peptides also reach the upper plateau (i.e. maximum signal) at the same time (~29.5 min.). This indicates that at this concentration there is likely a balance between the difference in surface activity of both peptides and the difference in the ensemble average populations of both folded and unfolded species in solution. Additionally, this result provides further insight into the vital role that charge distribution has on peptide adsorption dynamics as K-2.5 has a 31.9% ensemble average of α-helical species and K-6.0 has a 23% ensemble average of α-helical species, yet both peptides drive the system to the equivalent state at the same time.

Finally, at the concentrations of 0.41 μM and below, we see that there is a transition in the trend of the critical times where K-2.5 now has a lower critical time as compared to K-6.0. An explanation for this behavior is that K-2.5 maintains a greater

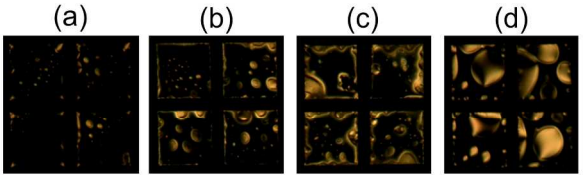

Figure 8. Heterogeneity across the LC/aqueous interface for K-2.5 at (a and b) 0.2 μM and (c and d) 0.4 μM.

population (+9%) of surface-active (folded) molecules than K-6.0. As mentioned above, previous studies have shown that peptides with localized charge distributσion occupy a smaller mean molecular area at a given surface pressure. In this regime (0.41 μM and below), K-6.0 remains capable of exerting a greater electrostatic repulsion between neighboring peptide molecules at the interface, however the population of amphipathic species is smaller. This result illustrates that our experimental configuration possesses a high degree of sensitivity, capable of detecting subtle differences in molecular structure that impacts both equilibrium and dynamic behavior.

Surface heterogeneities

The optical setup in Figure 1 is capable of examining the interfacial dynamics and equilibrium configurations of peptides adsorbed to an aqueous/liquid-crystal, surfactant-laden interface. The results presented thus far represent transitions from a purely homeotropic to planar orientation over the entire experimental area. However, at lower concentrations of only K-2.5, we observed coexistence of both planar and homeotropic domains (Figure 8 a-d). Figure 8 a and b shows this behavior at a peptide concentration of 0.2μM from two independent experiments. At this concentration small, spherical domains of planar orientation are visible surrounded by a homeotropic matrix. By doubling the concentration (Figure 8 c,d), we observed that the overall area occupied by the planar domains increased indicating the presence of a larger quantity of peptide at the interface. Price et al. observed similar findings using a similar setup in the presence of DNA hybridization at a surfactant-laden, LC/Aqueous [12]. These findings provided a framework for using the percentage of homeotropic coverage to determine the concentration of target in solution. Additionally, these observations further illustrate the uniqueness of this experimental setup as it is possible to visualize discrete differences in the path taken by two similar molecules to arrive at the same final equilibrium configuration.

Conclusions and Future Work

In this work, we examine the adsorption dynamics of two rationally designed peptide molecules using a LC-based experimental setup. The LC experimental platform shows sufficient sensitivity to optically observe molecular adsorption of two very similar molecules over macroscopic length scales. Analysis via circular dichroism was performed to determine the structural configurations of both molecules in solution and based on these findings examine the role of charged amino acid residue distribution on both structure and adsorption to a surfactant-laden interface. Both molecules were found to demonstrate tunable surface activity as a function of salt concentration. More specifically, for the case of equal quantities of folded peptides our

results suggest that peptides with more evenly distributed charges down the backbone have a stronger affinity for the LC/aqueous interface. Additionally, we were able to use this optical setup to obtain quantitative information about the system (i.e. critical transition concentration) and determine that our peptides follow a diffusion-limited adsorption mechanism. Further analysis also suggested no correlation between the rate of intensity change and the change in surface concentration as described by a simplified diffusion-limited model, likely owing to the time-scale differences between the peptide adsorption and surfactant rearrangement at the liquid crystal surface. Several instances of heterogeneous domain formation were also observed, suggesting that further optimization could be accomplished as previously described elsewhere [8, 12, 14].

Future studies will aim to address several key characteristics mentioned throughout this work, specifically: (1) optimize and further improve the sensitivity of the experimental setup to allow the detection of decreased analyte concentrations (2) examine the role that overall net charge has on the sensitivity and dynamics of interfacial adsorption by synthesizing "inverse" peptides with opposing charges at the same residue locations while keeping the surfactant constant (3) investigate the adsorption of peptides into insoluble layers (i.e. lipid monolayers) (4) obtain quantitative data to corroborate our findings from the analysis of optical images to measureable values (i.e. surface tension) via pendant bubble apparatus, and (5) probe the dynamics of specific, receptor-ligand protein interactions at the surface in an effort to move towards bio-sensing applications. Taken together, these studies aim to provide further insights into both the fundamental behavior of peptide/protein adsorption into surfactant layers and the development of this system for inexpensive and robust sensing applications.

Acknowledgments

This work was supported with funding from NSF (DMR - 1006407) and AFOSR (FA9550-14-1-0263). J.B. was partially supported from NSF (CBET - 0967365). C.B. was supported by the SloanFoundation (2011-6-11). We thank Nathan Lockwood for helpful discussions in the set up of the liquid crystal platform.

Notes and references

[a] *Department of Chemical Engineering, The City College of The City University of New York, New York, NY, USA. E-mail: tu@ccny.cuny.edu*

† Electronic Supplementary Information (ESI) available: [details of any supplementary information available should be included here]. See DOI: 10.1039/b000000x/

1 T. Ikeda, Journal of Materials Chemistry, 2003, 13, 2037-2057.
2 P. J. Collings, Hird, M, Introduction to Liquid Crystals: Chemistry and Physics, Taylor & Francis Ltd., USA, 1997.
3 M. Schadt, Annual Review of Materials Science, 1997, 27, 305-379.
4 D. S. Miller, R. J. Carlton, P. C. Mushenheim and N. L. Abbott, Langmuir, 2013, 29, 3154-3169.
5 N. A. Lockwood, J. J. de Pablo and N. L. Abbott, Langmuir, 2005, 21, 6805-6814.
6 J. M. Brake, M. K. Daschner, Y.-Y. Luk and N. L. Abbott, Science, 2003, 302, 2094-2097.
7 N. A. Lockwood, K. D. Cadwell, F. Caruso and N. L. Abbott, Advanced Materials, 2006, 18, 850-854.
8 A. C. McUmber, P. S. Noonan and D. K. Schwartz, Soft Matter, 2012, 8, 4335-4342.
9 Q.-Z. Hu and C.-H. Jang, Analyst, 2012, 137, 567-570.
10 J. M. Brake, M. K. Daschner and N. L. Abbott, Langmuir, 2005, 21, 2218-2228.
11 I. H. Lin, L. S. Birchall, N. Hodson, R. V. Ulijn and S. J. Webb, Soft Matter, 2013, 9, 1188-1193.
12 A. D. Price and D. K. Schwartz, Journal of the American Chemical Society, 2008, 130, 8188-8194.
13 A. M. Lowe and N. L. Abbott, Chemistry of Materials, 2011, 24, 746-758.
14 P. S. Noonan, R. H. Roberts and D. K. Schwartz, Journal of the American Chemical Society, 2013, 135, 5183-5189.
15 L. N. Tan, V. J. Orler and N. L. Abbott, Langmuir, 2012, 28, 6364-6376.
16 V. Nazarenko and A. Nych, Physical Review E, 1999, 60, R3495-R3497.
17 J. M. Brake and N. L. Abbott, Langmuir, 2002, 18, 6101-6109.
18 C. Kotsmar, V. Pradines, V. S. Alahverdjieva, E. V. Aksenenko, V. B. Fainerman, V. I. Kovalchuk, J. Krägel, M. E. Leser, B. A. Noskov and R. Miller, Advances in Colloid and Interface Science, 2009, 150, 41-54.
19 J. M. Rodríguez Patino, M. R. Rodríguez Niño and C. Carrera Sánchez, Current Opinion in Colloid & Interface Science, 2007, 12, 187-195.
20 J. V. Badami, P. Desir and R. S. Tu, Langmuir, 2014.
21 P. Y. Chou and G. D. Fasman, Biochemistry, 1974, 13, 222-245.
22 W. F. DeGrado and J. D. Lear, Journal of the American Chemical Society, 1985, 107, 7684-7689.
23 G. Xu, W. Wang, J. T. Groves and M. H. Hecht, Proceedings of the National Academy of Sciences, 2001, 98, 3652-3657.
24 V. Jain, A. Jimenez, C. Maldarelli and R. S. Tu, Langmuir, 2008, 24, 9923-9928.
25 V. P. Jain, C. Maldarelli and R. S. Tu, Journal of Colloid and Interface Science, 2009, 331, 364-370.
26 V. P. Jain and R. S. Tu, International Journal of Molecular Sciences, 2011, 12, 1431-1450.
27 L. Leon, P. Logrippo and R. Tu, Biophysical Journal, 2010, 99, 2888-2895.
28 L. Leon, W. Su, H. Matsui and R. Tu, Soft Matter, 2011, 7, 10285-10290.
29 E. Dickinson, Food Hydrocolloids, 2011, 25, 1966-1983.
30 J. M. Rodríguez Patino, M. R. Rodríguez Niño and C. C. Sánchez, Current Opinion in Colloid & Interface Science, 2003, 8, 387-395.
31 Q.-Z. Hu and C.-H. Jang, ACS Applied Materials & Interfaces, 2012, 4, 1791-1795.
32 Q.-Z. Hu and C.-H. Jang, Talanta, 2012, 99, 36-39.
33 N. A. Lockwood, J. K. Gupta and N. L. Abbott, Surface Science Reports, 2008, 63, 255-293.
34 J. T. Hunter and N. L. Abbott, Sensors and Actuators B: Chemical, 2013, 183, 71-80.

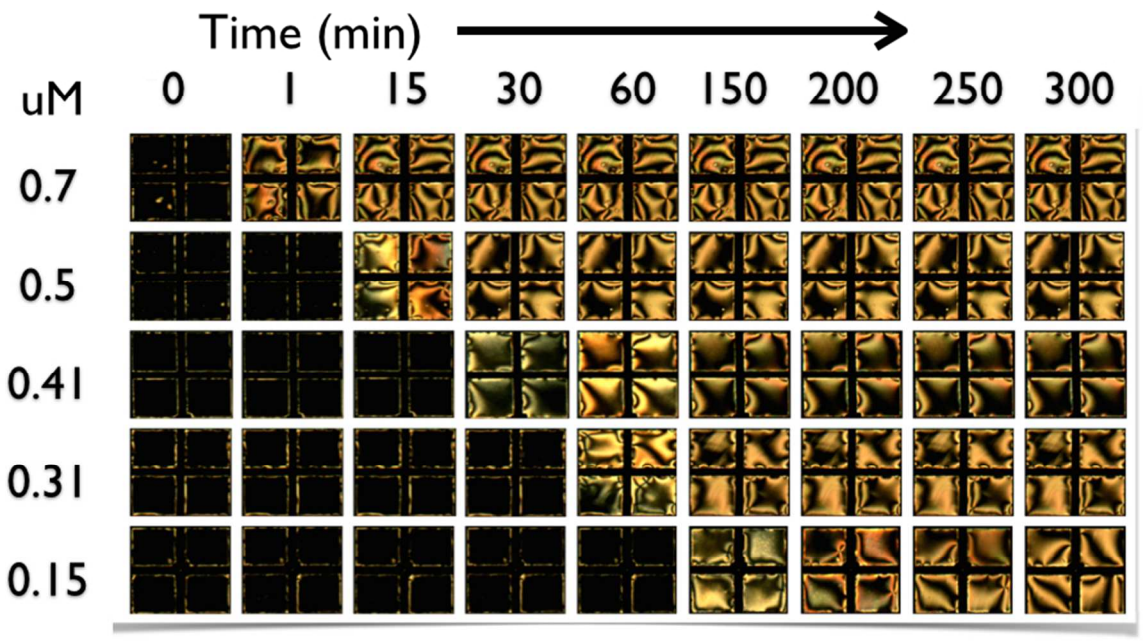

TOC. The liquid crystal platform provides a sensitive and quantitative tool for the detection of peptide adsorption kinetics.